Sound-Based Analogue of Cavity Quantum Electrodynamics in Silicon

Ö. O. Soykal, Rusko Ruskov, and Charles Tahan*

Laboratory for Physical Sciences, 8050 Greenmead Drive, College Park, Maryland 20740, USA

(Received 14 July 2011; published 28 November 2011)

A quantum mechanical superposition of a long-lived, localized phonon and a matter excitation is described. We identify a realization in strained silicon: a low-lying donor transition (P or Li) driven solely by acoustic phonons at wavelengths where high-Q phonon cavities can be built. This phonon-matter resonance is shown to enter the strongly coupled regime where the ''vacuum'' Rabi frequency exceeds the spontaneous phonon emission into noncavity modes, phonon leakage from the cavity, and phonon anharmonicity and scattering. We introduce a micropillar distributed Bragg reflector Si/Ge cavity, where $Q \simeq 10^5$–10^6 and mode volumes $\mathcal{V} \lesssim 25\lambda^3$ are reachable. These results indicate that single or many-body devices based on these systems are experimentally realizable.

DOI: 10.1103/PhysRevLett.107.235502 PACS numbers: 63.20.kd, 03.67.Lx, 42.50.Pq, 73.21.Cd

Cavity-quantum electrodynamics (cQED) refers to the interaction of a single mode of the electromagnetic field with a dipole emitter. cQED has provided new ways of controlling photons and matter (atoms, qubits, etc.) in both atomic and solid-state systems. The progression from an atom ''dressed'' with a cavity photon (''traditional'' cavity QED) [1,2] to a semiconductor microcavity polariton (exciton plus cavity photon) [3] to solid-state many-body polaritonic devices [4–6] has opened up new avenues for physical investigation as well as technology (e.g., single photon sources, novel lasers, long-range entanglement, quantum simulation). Motivated by this, we seek an analogous progression utilizing quantum sound instead of light.

Phonons are more suitable for some tasks than photons due to their slower speeds and smaller wavelengths (e.g., in signal processing, sensing, or nanoscale imaging). Our work builds off recent experimental results in nano-optomechanical systems [7], where cooling, coherent control, and lasing of mechanical vibrations have been achieved, as well as previous consideration of phonons as decoherence pathways [8], as tools for coupling quantum systems [9–11], and even as a means for simulating many-body dynamics [12].

In this Letter, we show that a phonon-based analogue of the cavity polariton is possible. Introducing a suitable high-Q phonon cavity, we calculate the cavity-phonon coupling to a two-level system (TLS) in silicon (Fig. 1) and also losses due to spontaneous phonon emission from the donor into noncavity modes, phonon leakage from the cavity, and phonon anharmonicity and scattering. Despite the phonon's dependent nature on its host material and the different (nondipole) donor-phonon interaction, a strong coupling regime can be established, similar to cQED, where the phonon-TLS states are hybridized. The result of this mixing of cavity phonon and matter excitation we term the cavity *phoniton* [13].

Implementation.—Silicon is a promising candidate for constructing a cavity-phoniton system. The physics of shallow donors in Si have been understood since the 1950s and experimentally verified, while transitions between low energy donor states are known to be driven by acoustic phonons [15]. The sixfold degeneracy due to Si's multivalley conduction band is lifted both by applied strain (e.g., due to the lattice mismatch with a substrate) and the sharp donor potential. Crucially, in [001] compressively strained Si (Fig. 1), the first excited state at zero magnetic field of a phosphorous donor approaches $\Delta_v^P \simeq 3.02$ meV (0.73 THz): a so-called excited ''valley'' state. (The excited valley state has an s-like envelope function like the ground state but opposite parity; because of this, valley state relaxation times can be much longer than for charge states.) The energy splitting implies longitudinal (transverse) wavelengths of $\lambda_l \approx 12.3$ nm ($\lambda_t \approx 7.4$ nm). For comparison, the energy splitting to the upper $2p$-like state is >30 meV ($\lambda_{2p} \approx 1.2$ nm), unlikely to be amenable to phonon cavities. Since the P:Si Bohr radius is $a_B^* \lesssim 2.5$ nm

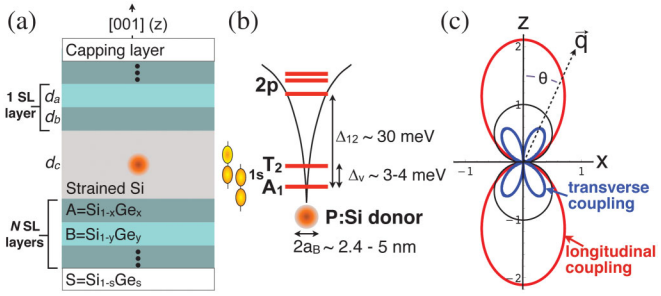

FIG. 1 (color). (a) A cavity phoniton can be constructed in a Si/Ge heterostructure cavity as a hybridized state of a trapped single phonon mode and a donor TLS placed at a maxima of the phonon field. (b) The P:Si donor lowest $1s$ valley states, A_1, T_2, and upper levels ($1s/2p$); their energy splittings can be controlled by the applied strain in the Si cavity. (c) Angular dependence of the coupling $g_q(\theta)$, Eq. (2), for the deformation potentials of Ref. [16] versus dipole $\sim \cos\theta$ dependence (thin circles).

in the bulk, $\lambda > a_B^*$ allows for easier donor placement, avoidance of interface physics, and bulklike wave functions.

A prototype implementation of a cavity-phoniton system in silicon is sketched in Fig. 1(a). A strained-Si phonon cavity grown in the [001] direction, of length $d_c \sim \lambda$ and lateral size D, is enclosed by acoustic distributed Bragg reflectors (DBRs) formed as layered, epitaxially grown, and strain-relaxed SiGe super lattice (SL) heterostructures. The cavity length is chosen to be less than the critical thickness due to strain (see, e.g., Ref. [17]). The DBR SL unit periods consist of subsequent layers $(A, B) = \mathrm{Si}_{1-x_{A,B}}\mathrm{Ge}_{x_{A,B}}$ of thickness (d_A, d_B), strain matched to a $\mathrm{Si}_{1-s}\mathrm{Ge}_s$ substrate [$x_{A(B)} = 0.55(0.05)$, $s = 0.26$, maximizing confinement], and an appropriate capping layer, depending on the actually confined phonon mode. Note that 1D DBR SL phonon cavities ($D \gg d_c$) are well understood and have been demonstrated in THz phonon cavities in III-V's [7,18]; coherent phonons in SiGe superlattices were studied as well [19]. In the case of micropillar DBR (mpDBR) structures (designed to increase the phonon-donor coupling), the DBR lateral dimension may become comparable to the phonon wavelength ($D \gtrsim d_c \sim \lambda$) and the confined mode is a mixed longitudinal and transverse one. The trapped mode with wavelength λ_q and phase velocity v_q is designed to be resonant in energy with the first excited state of the donor. Similar to the 1D DBR [20], the thickness of the SL unit cell is set to match the Bragg condition $d_{A,B}^{(q)} = v_{A,B}^{(q)}\lambda_q/4v_q$, where $v_{A,B}^{(q)}$ are the phase velocities (using isotropic approximation, see, e.g., Ref. [21]). The donor is placed at the center of a λ cavity ($d_c = \lambda_q$), where the displacement $\boldsymbol{u}(\boldsymbol{r})$ is maximal [22].

Hamiltonian and coupling.—In the semiclassical picture an acoustic phonon creates a time-dependent strain, $\varepsilon_{\alpha\beta}(\boldsymbol{r}) = \frac{1}{2}(\frac{\partial u_\alpha}{\partial r_\beta} + \frac{\partial u_\beta}{\partial r_\alpha})$, which modulates the energy bands and can drive transitions in a localized state, e.g., a donor. For Si, from the multivalley electron-phonon interaction [14,16] one can derive the matrix element between valley states, $|s, j\rangle$:

$$V_{ij}^{s's} \equiv \hbar g_{\boldsymbol{q}} = i\langle s', i|\Xi_d \,\mathrm{Tr}(\varepsilon_{\alpha\beta}) + \tfrac{1}{2}\Xi_u\{\hat{\boldsymbol{k}}_i^\alpha\hat{\boldsymbol{k}}_i^\beta + \hat{\boldsymbol{k}}_j^\alpha\hat{\boldsymbol{k}}_j^\beta\}\varepsilon_{\alpha\beta}|s, j\rangle, \quad (1)$$

where $\hat{\boldsymbol{k}}_{i,j}$ are the directions toward the valleys, s, s' label the orbital (envelope) function(s), and $\Xi_u(\mathrm{Si}) \simeq 8.77$ eV, $\Xi_d(\mathrm{Si}) \approx 5$ eV [16] are deformation potential constants. For the donor-phonon Hamiltonian we obtain the interaction (of Jaynes-Cummings type) $H_g \approx \hbar g_{\boldsymbol{q}}(\sigma_{ge}^+ b_{\boldsymbol{q},\sigma} + \sigma_{ge}^- b_{\boldsymbol{q},\sigma}^\dagger)$, where only the resonant cavity phonon with quantum numbers $\boldsymbol{q}, \sigma$ and energy $\hbar\omega_{\boldsymbol{q},\sigma}$ is retained, $b_{\boldsymbol{q},\sigma}^\dagger$ is the phonon creation operator, and $\sigma_{ge}^+ \equiv |e\rangle\langle g|$ refers to the donor transition between ground and excited states [23]. In the loss part, $H_{\mathrm{loss}} = H_\kappa + H'_{\mathrm{anh}} + H_\Gamma$, H_κ couples the cavity mode to external continuum of other modes giving a cavity decay rate $\kappa = \omega_{\boldsymbol{q},\sigma}/Q$ (expressed through the Q factor), H'_{anh} includes phonon decay due to phonon self-interaction and also phonon scattering off impurities (mainly mass fluctuations in natural Si). The coupling of the donor to modes other than the cavity mode H_Γ leads to its spontaneous decay.

The valley states, $1s(A_1)$, $1s(T_2)$, that make up the TLS are the symmetric and antisymmetric combinations of the conduction band valley minima along the $\hat{z}$ direction [see Fig. 1(b)]. Because of opposite parity of the states, the intravalley contributions cancel. The intervalley transitions are preferentially driven by umklapp phonons [24] with a wave vector $\boldsymbol{q}$ at $q_u \simeq 0.3\frac{2\pi}{a_0}$, where $\boldsymbol{q}_u \equiv \boldsymbol{G}_{+1} - 2\boldsymbol{k}_{\hat{z}}$ is the wave vector "deficiency" of the intervalley $\boldsymbol{k}_{\hat{z}} \to -\boldsymbol{k}_{\hat{z}}$ transition, and $\boldsymbol{G}_{+1} = \frac{4\pi}{a_0}(0, 0, 1)$ is the reciprocal vector along $\hat{z}$. Since typical values give $q_u r \approx q_u a_B^* \simeq 9.4 > 1$ and $qr \sim 1$ for 3 meV, the coupling is calculated exactly (not using the dipole approximation) for longitudinal and transverse polarizations

$$g_{\mathbf{q}}^{(\sigma)} = \left(\frac{a_G^2 q^2}{2\rho\hbar\mathcal{V}\omega_{\boldsymbol{q},\lambda}}\right)^{1/2} I^{ge}(\theta)\begin{cases}\Xi_d + \Xi_u\cos^2\theta & [l]\\ \Xi_u\sin\theta\cos\theta & [t],\end{cases} \quad (2)$$

where $a_G \approx 0.3$, $I^{ge}(\theta) = \int d\boldsymbol{r}[\Phi_{1s}^{\hat{z}}(\boldsymbol{r})]^2 e^{-i\boldsymbol{q}\boldsymbol{r}}\sin(\boldsymbol{q}_u\boldsymbol{r}) = [2\beta_q\cos\theta(1-\gamma_q\cos^2\theta)]/\{\alpha_q^2[(1-\gamma_q\cos^2\theta)^2 - \beta_q^2\cos^2\theta]^2\}$ is the intervalley overlapping factor, $\alpha_q = 1 + \frac{1}{4}(q^2a^2 + q_u^2b^2)$, $\beta_q = \frac{1}{2\alpha_q}b^2qq_u$, $\gamma_q = \frac{1}{4\alpha_q}(a^2 - b^2)q^2$, and a/b are the radii of the Kohn-Luttinger envelope function $\Phi_{1s}^{\hat{z}}(\boldsymbol{r})$ (see, e.g., Ref. [16]). The calculated coupling is to plane wave modes, related to a rectangular cavity with periodic boundary conditions. Figure 1(c) shows the directionality of the coupling for longitudinal and transverse phonons. The angular dependence in Eq. (2) for longitudinal phonons is similar to dipole emission ($I_{\mathrm{dip}}^{ge} \sim \cos\theta$), but enhanced in a cone around the $\hat{z}$ direction due to nondipole contributions. Uncertainties in Ξ_d calculations (see Ref. [25]) result in an overall factor of 2 difference in the maximal coupling.

Coupling to cavity mode.—The matrix element $\hbar g_{\mathbf{q}}^{(\sigma)}$ is just the interaction energy of the donor with the "phonon vacuum field" and expresses a generic dependence $\propto 1/\sqrt{\mathcal{V}}$ on the normalization volume; it goes to zero for large volumes. In a cavity, $\mathcal{V}$ is the physical volume of the mode [26]. By virtue of Eq. (2), we first consider a DBR cavity with a length $d_c = \lambda_l \simeq 12.3$ nm designed for longitudinal resonant phonon along the z direction (we use isotropic velocities for Si, $v_l = 8.99 \times 10^3$ m s^{-1}, $v_t = 5.4 \times 10^3$ m s^{-1}, see Ref. [21]). Taking the minimal lateral size $D_{\min} \approx \lambda_l$ to ensure $D > 2a_B^* \approx 5$ nm, one gets a mode volume of $\mathcal{V}_{\min} \approx \lambda^3$ for P:Si. Thus, we estimate the maximal phonon-donor coupling as $g_{1\lambda} = 3.7 \times 10^9$ s^{-1}. For $D = 5\lambda$ the coupling is still appreciable: $g_{5\lambda} = 7.4 \times 10^8$ s^{-1}. Surface undulation typical of step-graded SiGe quantum wells (see Ref. [17]) gives

$D \approx 200$ nm $\lesssim 15\lambda$, though this interface imperfection is avoidable with heterostructures grown on defect-free nanomembrane substrates [27].

For a realistic cylindrical mpDBR cavity, the modes can be constructed as standing waves with energy $\hbar\omega$ and wave number q along the pillar z direction, with stress-free boundary conditions on the cylindrical surface. The displacements for compressional modes (see, e.g., Ref. [28]) are $u_r(r,z) = [A_r J_1(\eta_l r) + B_r J_1(\eta_t r)]\sin qz$, $u_z(r,z) = [A_z J_0(\eta_l r) + B_z J_0(\eta_t r)]\cos qz$, where $J_{0,1}(r)$ are Bessel functions of the first kind, $\eta_{l,t} \equiv \sqrt{\omega^2/v_{l,t}^2 - q^2}$, and A_i, B_i are constants. These modes are lower in energy and couple strongly to the donor; the related strain has a node at the Si-cavity z boundaries (for λ cavity) [22]. For a fixed resonant frequency ω and lateral size D, the dispersion relation $q = \omega/v_q(D)$ has multiple solutions q_i, $i = 0, 1, 2, \ldots$, where q_0 stands for the fundamental mode, q_1 for the 1st excited mode, etc. Each mode propagates with its own phase velocity $v_{q_i}(D) \neq v_l, v_t$. For a λ cavity and $D = \lambda_l$ we calculate via Eq. (1) maximal coupling to the fundamental mode with $\lambda_{q_0} = 6.9$ nm to be $g_{1\lambda}^{(0)} = g_{\max} = 6.5 \times 10^9$ s^{-1} (see Table I), comparable to the above estimation. For larger D, however, the coupling to the fundamental mode rapidly decreases (e.g., $g_{5\lambda}^{(0)} = 5.8 \times 10^5$ s^{-1}) since the mode transforms to a surfacelike Rayleigh wave ($v_{\text{Rayleigh}} < v_t$). Coupling to higher mode branches is appreciable and decreases roughly as $1/\sqrt{V}$, e.g., for the 1st mode branch, $g_{1\lambda}^{(1)} = 2.4 \times 10^9$ s^{-1} and $g_{5\lambda}^{(1)} = 3 \times 10^8$ s^{-1}. Among various mode choices we note that for any diameter D there is a higher excited mode with resonant wavelength close to that for longitudinal phonons. For example, for $D = 3\lambda_l$ we found the wavelength of the resonant 4th excited mode as $\lambda_{q_4} \simeq 12.4$ nm and the coupling $g_{3\lambda}^{(4)} = 3 \times 10^9$ s^{-1} (i.e., values similar to the rectangular DBR estimate).

Loss.—Losses in this system are dominated by donor relaxation and leakage of the confined phonon mode. Similar to cQED (see, e.g., Ref. [26]), one can argue that the donor relaxation Γ_{relax} to modes different than the cavity mode (and generally not trapped into the cavity) is bounded by the donor spontaneous emission rate in the bulk: $\Gamma_{\text{relax}} \lesssim \Gamma$. We calculated the bulk donor relaxation to longitudinal and transverse phonons to be $\Gamma_{ge}^{(l)} = 3 \times 10^7$ s^{-1} and $\Gamma_{ge}^{(t)} = 9.2 \times 10^7$ s^{-1}, respectively, for the 3 meV transition ($\Gamma = \Gamma_{ge}^{(l)} + \Gamma_{ge}^{(t)} = 1.2 \times 10^8$ s^{-1}). The relaxation to photons is electric dipole forbidden and suppressed [16] by $(\lambda_{\text{photon}}/a_B^*)^2 \sim 10^{10}$.

The cavity mode loss rate is calculated as mainly due to leakage through the DBR mirrors, similar to optical DBR cavities [31] (except that for phonons there is no leakage through the sides). Generally, for the cylindrical micropillar DBRs, the cavity mode involves coupled propagation along the micropillar of two displacement components, $u_z(r,z)$, $u_r(r,z)$, and two stress fields, T_{zz}, T_{zr}. For small diameters, $D \ll \lambda_l$, the fundamental mode becomes mainly longitudinal ($\sim u_z$), propagating with the Young velocity, $v_0 = \sqrt{E/\rho}$. Using 4×4 transfer matrices we calculated $Q_{\text{mpDBR}}^{(0)} \simeq 10^6$ for $N = 33$ layers for the confined, mixed fundamental mode at $D = \lambda_l$, which is close to the limiting Q factor related to pure longitudinal propagation [32]. (This is also similar to the 1D DBR value relevant for $D \gg \lambda_l$.) For our design we obtain a cavity loss rate $\kappa = \Delta_v/\hbar Q \simeq 2.8 \times 10^6$ s^{-1}. This can be decreased by adding more layers.

At low temperatures the phonon anharmonicity losses are negligible (a rate $\Gamma_{\text{anh}} \simeq 1.4 \times 10^4$ s^{-1} at 3 meV), while scattering off impurity mass fluctuations in natural Si amounts to a rate 2 orders of magnitude larger: $\Gamma_{\text{imp}} \approx 7 \times 10^5$ s^{-1}. It is notable that in isotopically purified bulk silicon (an enrichment of ^{28}Si to 99%) the scattering rate will decrease by an order of magnitude and the related phonon mean free path will be of the order of $v_l/\Gamma_{\text{imp}} \approx 10$ cm [28,33,34]. In this case, the cavity leakage dominates, $\kappa \gg \{\Gamma_{\text{anh}}, \Gamma_{\text{imp}}\}$, and the number of vacuum Rabi flops can reach as high as $n_{\text{Rabi}} = 2g(D)/(\Gamma + \kappa) \simeq 102$ for a cavity Q factor, $Q = 10^6$, and some $n_{\text{Rabi}} \simeq 77$ for $Q = 10^5$. For $D = 10\lambda_l$ and similar Q one still has $n_{\text{Rabi}}^{(1)} \simeq 1(17)$ for the 1st (2nd) excited mode. Further, nearby modes can be well separated from the resonant mode, e.g., for the fundamental mode and $D = \lambda_l$ the next mode (in transverse direction) is $\sim 0.3\Delta_v = 0.9$ meV off; the transverse separation for $D = 10\lambda_l$ (for the 1st excited

TABLE I. Key rates and parameters for circuit QED [29] (1D cavity) versus the phoniton system; we show calculations for maximal coupling for a λ cavity with lateral diameter of $D = \lambda_l$ (in general, $g \sim 1/\sqrt{V}$), $Q = 10^6$, and comparable number of Rabi flops [30].

Parameter	Symbol	Circuit QED	P:Si phoniton	Li:Si phoniton
Resonance frequency	$\omega_r/2\pi$	10 GHz	730 GHz	142 GHz
Vacuum Rabi frequency	g/π	100 MHz	2.1 GHz	13.8 MHz
Cavity lifetime	$1/\kappa$, Q	160 ns, 10^4	0.22 μs, 10^6	1.1 μs, 10^6
TLS lifetime	$1/\Gamma$	2 μs	8.2 ns	22 μs
Critical atom number	$2\Gamma\kappa/g^2$	$\lesssim 6 \times 10^{-5}$	$\lesssim 3 \times 10^{-5}$	$\lesssim 4 \times 10^{-5}$
Critical phonon number	$\Gamma^2/2g^2$	$\lesssim 10^{-6}$	$\lesssim 2 \times 10^{-4}$	$\lesssim 6 \times 10^{-7}$
Number of Rabi flops	$2g/(\kappa + \Gamma)$	$\sim$100	$\sim$102	$\sim$93

mode) gives $0.009\Delta_v$, which is more than 2 orders of magnitude larger than the linewidth $\Gamma_0 \simeq (\Gamma + \kappa)/2$ of the two hybridized levels.

Experiment and discussion.—We have shown that the donor:Si cavity phoniton can enter the strong coupling regime with $2g/(\Gamma + \kappa) \sim 10$–$100$ (Table I). A principle experimental confirmation would be the observation of the vacuum Rabi splitting: $\Omega_0 = [g^2 - (\Gamma - \kappa)^2/4]^{1/2}$; two resolved spectral peaks can be observed if $2\Omega_0 > \Gamma_0$. The Rabi splitting can be enhanced as $\Omega_0 \simeq g\sqrt{N}$ by placing more than one donor ($N > 1$) in the cavity [1,26] (e.g., via a delta-doped layer). This could allow for large coupling even for large diameter micropillars or 1D DBR structures (since $\frac{\sqrt{N}}{\sqrt{V}} \propto \frac{\sqrt{D^2}}{D} = 1$). Further, strain or electric field (from a top gate) [10,35,36] can be used to tune the valley transition into resonance.

Experimental techniques are available to probe the Si-phoniton (low temperature, $T \sim 1$ K, and low phonon numbers are assumed). First, free-electron lasers have been used to probe the $1s$-$2p$ transitions in P:Si [37]. Observation of the vacuum Rabi splitting is possible by measurement of the absorption spectrum of the allowed optically probed transition $1s(T_2) \rightarrow 2p_0$ (~ 30 meV) using weak optical excitation. Appropriate phonons can be introduced to the system by excited valley state emission, by piezoactuators, or by increasing the temperature, as was done for the first observations of Rabi oscillations [38] (phonons of 3 meV ~ 30 K). Second, pump and probe optical techniques have been demonstrated to observe coherent phonon effects in III-V [7,18] and SiGe [19] SL heterostructures. Observing the reflected phonons from this structure will show the phonon-Rabi splitting characteristic of cavity-QED systems [1].

The cavity phoniton can be realized in other materials and systems. In particular, our system should be compatible with recently demonstrated (though in the few GHz range) high-Q phononic band-gap nanomechanical and optomechanical (membrane) cavities in silicon (e.g., in [7,39]). Quantum dots, spin transitions, color centers in diamond, and other donors (particularly Li:Si [10]) may offer smaller resonance energies and correspondingly larger cavities (wavelengths) [34]. In the case of [001]-strained Si considered in this Letter, the two lowest levels in Li possess essentially the same state structure as P:Si and approach a splitting of $\Delta_{\mathrm{Li}} = 0.586$ meV for high strain (from zero splitting at no strain). We calculate (see Table I) the corresponding Li:Si donor-phonon coupling for the $D = \lambda_l$ (now $\lambda_l = 63.2$ nm) reference cavity; strong coupling can still be reached. For the DBR cavities, the Si critical thickness can be made 80–100 nm by lowering the Ge content in the substrate. For 2D-phononic band-gap cavities, direct numerical calculations for cavity-trapped phonons ($\omega_r/2\pi \approx 10$ GHz) in novel Si nanostructures [39] show the potential to reach $Q_{\mathrm{cav}} \gtrsim 10^7$ in the ideal case.

The phoniton is a new component for constructing and controlling macroscopic artificial quantum systems based on sound. Besides single phonon devices, systems composed of many coupled phonitons could exhibit novel quantum many-body behavior. For example, "solid-sound" systems in analogy with coupled cavity-QED solid-light systems [5] could demonstrate Mott-insulator-like states of phonons in coupled phoniton cavities. Cavity or qubit geometries such as these may also be relevant for quantum computing applications: to mediate interactions between distant qubits or inhibit decoherence. The systems proposed here will benefit from the drive in silicon quantum computing towards more purified materials, perfect surfaces, and precise donor placement.

Special thanks to Chris Richardson for input on realistic SiGe heterostructures and to Ari Mizel, Robert Joynt, and Mark Friesen for valuable discussion. This work was funded in part by DARPA.

*charlie@tahan.com

[1] H. J. Kimble, Phys. Scr. **T76**, 127 (1998).
[2] J.-M. Raimond, M. Brune, and S. Haroche, Rev. Mod. Phys. **73**, 565 (2001).
[3] Y. Yamamoto, F. Tassone, and H. Cao, *Semiconductor Cavity Quantum Electrodynamics* (Springer, Berlin, 2000).
[4] P. Littlewood, Science **316**, 989 (2007).
[5] A. D. Greentree *et al.*, Nature Phys. **2**, 856 (2006).
[6] A. Kavokin and G. Malpuech, *Cavity Polaritons* (Elsevier, Amsterdam, 2003), Vol. 32.
[7] A. J. Kent *et al.*, Phys. Rev. Lett. **96**, 215504 (2006); C. A. Regal *et al.*, Nature Phys. **4**, 555 (2008); M. Eichenfield *et al.*, Nature (London) **462**, 78 (2009); A. K. Huttel *et al.*, Nano Lett. **9**, 2547 (2009); T. Rocheleau *et al.*, Nature (London) **463**, 72 (2009); R. P. Beardsley *et al.*, Phys. Rev. Lett. **104**, 085501 (2010); A. D. O'Connell *et al.*, Nature (London) **464**, 697 (2010); A. Bruchhausen *et al.*, Phys. Rev. Lett. **106**, 077401 (2011).
[8] A V. Khaetskii and Y. V. Nazarov, Phys. Rev. B **64**, 125316 (2001); C. Tahan, M. Friesen, and R. Joynt, Phys. Rev. B **66**, 035314 (2002); I. Wilson-Rae and A. Imamoğlu, Phys. Rev. B **65**, 235311 (2002).
[9] J. I. Cirac and P. Zoller, Phys. Rev. Lett. **74**, 4091 (1995).
[10] V. N. Smelyanskiy, A. G. Petukhov, and V. V. Osipov, Phys. Rev. B **72**, 081304(R) (2005).
[11] P. Rabl *et al.*, Phys. Rev. B **79**, 041302(R) (2009).
[12] D. Porras and J. I. Cirac, Phys. Rev. Lett. **93**, 263602 (2004).
[13] The phoniton involves a short-range electron-acoustic-phonon interaction (in a nonpolar crystal). The term polaron has been reserved for a propagating electron plus the (long-range [14]) polarization field (usually optical phonons) in an ionic crystal.
[14] G. L. Bir and G. E. Pikus, *Symmetry and Strain-Induced Effects in Semiconductors* (Keter Publishing House, Jerusalem, 1974).
[15] D. Wilson and G. Feher, Phys. Rev. **124**, 1068 (1961).

[16] P. Yu and M. Cardona, *Fundamentals of Semiconductors* (Springer, Berlin, 2010).
[17] K. Brunner, Rep. Prog. Phys. **65**, 27 (2002).
[18] M. Trigo *et al.*, Phys. Rev. Lett. **89**, 227402 (2002).
[19] Y. Ezzahri *et al.*, Phys. Rev. B **75**, 195309 (2007).
[20] S. M. Rytov, Akust. Zh. **2**, 71 (1956) [Sov. Phys. Acoust. **2**, 68 (1956)].
[21] S. M. Komirenko *et al.*, Phys. Rev. B **62**, 7459 (2000).
[22] The intervalley transition $1s(A_1) \rightarrow 1s(T_2)$ gives an odd in z contribution, Eq. (2), that overlaps with the strain, since at maximum $\boldsymbol{u}(\boldsymbol{r})$ strain changes sign.
[23] See Supplemental Material at http://link.aps.org/supplemental/10.1103/PhysRevLett.107.235502 for a derivation of the phoniton Hamiltonian, donor-phonon coupling, cavity design and properties, and losses.
[24] T. G. Castner, Phys. Rev. **130**, 58 (1963).
[25] P. W. Leu, A. Svizhenko, and K. Cho, Phys. Rev. B **77**, 235305 (2008).
[26] P. R. Berman, *Cavity Quantum Electrodynamics* (Academic, Boston, 1994).
[27] D. M. Paskiewicz *et al.*, ACS Nano **5**, 5814 (2011).
[28] A. N. Cleland, *Foundations of Nanomechanics* (Springer, Berlin, 2003).
[29] A. Blais *et al.*, Phys. Rev. A **69**, 062320 (2004).
[30] For 3D-optical or microwave cavities [1,2], the number of Rabi flops is limited by the finite transit time.
[31] M. Pelton *et al.*, IEEE J. Quantum Electron. **38**, 170 (2002).
[32] For a 1D DBR cavity we evaluate $Q_{\mathrm{DBR}} \simeq 2\pi(d_c + L_{\mathrm{DBR}})\sqrt{R_c}/\lambda \ln R_c$, where $L_{\mathrm{DBR}} = Z_A Z_B \lambda_q / 2Z_c |Z_B - Z_A|$ is the acoustic DBR mirror length and $R_c = [(Z_s/Z_c - Z_r^{2N})/(Z_s/Z_c + Z_r^{2N})]^2$ is the peak power reflectivity for N layers with impedance ratio $Z_r = \rho_A v_A / \rho_B v_B$ (Z_s and Z_c are the impedances of the substrate and cavity, respectively).
[33] K. Schwab *et al.*, Nature (London) **404**, 974 (2000).
[34] For long enough wavelengths one can neglect roughness effects in the phonon surface reflection as indicated in thermal conductance experiments [33] (see also [28]).
[35] M. Friesen, Phys. Rev. Lett. **94**, 186403 (2005).
[36] G. P. Lansbergen *et al.*, Nature Phys. **4**, 656 (2008); L. Dreher *et al.*, Phys. Rev. Lett. **106**, 037601 (2011).
[37] P. T. Greenland *et al.*, Nature (London) **465**, 1057 (2010).
[38] G. Rempe, H. Walther, and N. Klein, Phys. Rev. Lett. **58**, 353 (1987).
[39] A. H. Safavi-Naeini and O. Painter, Opt. Express **18**, 14926 (2010).